Improved EIT drive patterns for a robotics sensitive skin

David Silvera Tawil, David Rye and Mari Velonaki
Centre for Social Robotics/Australian Centre for Field Robotics
The University of Sydney, Australia
{d.silvera|d.rye|m.velonaki}@acfr.usyd.edu.au

Abstract

Electrical impedance tomography (EIT) is a technique used to estimate the internal conductivity of an electrically conductive body by using only measurements from its boundary. If this body is made of a thin, flexible and stretchable material that responds to touch with local changes in conductivity, it can be used to create an artificial sensitive skin. Mathematically, the EIT reconstruction problem is an ill-posed nonlinear inverse problem in which it is commonly assumed that electrodes are only located on the boundary. In a thin sensitive skin, however, electrodes can readily be located within the body. This paper compares existing drive patterns with new patterns in which a reference electrode is located inside the body. Simulation results demonstrate that placing a reference electrode in the centre of the body can improve both the resolution and robustness to noise of the reconstructed image.

1 Introduction

As the capability of robots grows, there is an increasing interest in building robots that can interact with humans in more natural ways; for example Kismet [Breazeal, 2003] is a robotic 'creature' that displays and 'understands' expressive emotions. Robots such as the FishBird wheelchairs [Velonaki *et al.*, 2005] have demonstrated that people naturally seek interaction through touch and expect robots to respond to tactile stimulus. Researchers have developed robots with a basic 'understanding' and/or reaction to touch for therapy through affective touch; some examples are Paro the seal [Wada *et al.*, 2002], the Huggable [Stiehl and Breazeal, 2005] and Hapticat [Yohanan *et al.*, 2005]. These robots do not closely resemble real animals, thus reducing the pitfalls of the uncanny valley [Mori, 1970].

Touch is the largest of all human senses and the first one to develop. Our bodies are literally covered by millions of different touch receptors; our muscles, joints and organs are all connected to nerves that constantly send information to the brain. Almost everything we do, including walking, talking, sitting and kissing depends on touch; it is almost impossible to imagine life without it.

The interpretation of touch between humans is highly complex and is strongly dictated by the context of the interaction, along with the communicator's culture, emotions, and beliefs [McDaniel and Andersen, 1998]. Early work on social interaction [Heslin, 1974] demonstrated that humans extract certain characteristics from tactile stimuli that communicate different messages, and that interpretation of touch is affected by factors such as modality (pat, squeeze, brush, stroke, poke, etc.), location, duration, intensity and frequency of touch.

In robotics it is important to design a method for touch identification that can be active over all or most of the robot's body area; this could be done though an artificial sensitive skin. The functional requirements for an artificial sensitive skin are debatable, and to some extent must be dependent on the robot's application. In the literature, an artificial sensitive skin is usually regarded as a flexible [Minato *et al.*, 2007], stretchable [Hoshi and Shinoda, 2006] array of sensors that fits onto curved robot surfaces of substantial extent and has the ability to sense tactile information such as pressure [Shimojo *et al.*, 2004], proximity [Stiehl and Breazeal, 2005], temperature [Stiehl and Breazeal, 2005], slip and texture. The skin could be soft [Mukat, 2004] and should feel 'good' when touched. For a robotics implementation, all hardware must be embedded in the robot and software must execute in real time.

From the first comprehensive elucidation of the concept of 'sensitive skin' by Vladimir Lumelsky [2001], robotics researchers have contributed several prototypes of artificial skin that usually consist of a number of discrete sensors [Mukai *et al.*, 2008] connected individually or in a grid configuration [Papakostas *et al.*, 2002], capable of responding to touch, temperature [Stiehl and Breazeal, 2006] and other physical phe-

nomena. Approaches to sensing range from the use of organic field-effect transistors (OFETs) [Someya *et al.*, 2006] or piezoresistive semiconductors [Mukai *et al.*, 2008] to transducers that use capacitance [Chang *et al.*, 2006], piezoelectricity [Ishiguro and Nishio, 2007] or optics [Nicholls, 1991], to the recent use of electrical impedance tomography [Kato *et al.*, 2007].

Electrical impedance tomography (EIT) [Holder, 2005] is an imaging technique used to estimate the internal conductivity of an electrically conductive body by using only measurements made at the boundary of the body. If the conductivity in a region of the body changes, the current distribution also changes and EIT can be applied to quantify these changes. The application of EIT to sensitive skin was previously described by Kato *et al.* [2007], Nagakubo *et al.* [2007] and Alirezaei *et al.* [2009]. These researchers located electrodes on the border of a rubberised fabric that responds to applied pressure with local changes in resistivity. By applying EIT, changes in resistance—and therefore pressure—can be identified. Since most of the sensing area is made of a homogeneous thin material without any wiring, a flexible and stretchable 'skin' can be realised.

Mathematically, the EIT reconstruction problem is an ill-posed nonlinear inverse problem, in which the main complication is that the reconstructed image is not necessarily a unique and stable solution: small changes in the data (e.g. electrical noise) can cause large changes in the reconstruction. A common assumption is that electrodes are only located on the boundary; in a thin sensitive skin, however, electrodes can easily be located within the body as well as on the boundary. This paper compares different patterns of current excitation and potential measurement that have been used, and introduces new patterns in which a reference electrode is located inside the body of a sensitive skin. Simulation results demonstrate that an electrode at the centre of the body improves both the resolution of the reconstructed image and its stability in the presence of noise.

2 Electrical impedance tomography

EIT is a technique used principally in medical imaging to estimate the internal conductivity of regions within a human body by using only measurements made on the person's skin. Typically, multiple electrodes are placed on a person's thorax and a small alternating current is applied across two of the electrodes. Current will flow not only between the two driving electrodes but also within the whole conductive body; the potentials resulting at all electrodes are measured. Local variations in the internal conductivity of the body alter the current pathways, resulting in changes of potential at the boundary. By repeating these steps and scanning around various electrode pairs it is possible to calculate the approximate current distribution inside the body through inverse solution of Maxwell's equations. A medical image can be constructed since different structures within the human body have different resistivities. If direct current is used instead of AC and the same method applied, the technique is called electrical resistive tomography (ERT).

The EIT reconstruction problem is to find the conductivity inside an object when a set of injected currents and the resulting potentials are known. The first method proposed for reconstruction was back-projection [Barber *et al.*, 1992], a linear, non-iterative method in which the equipotential volume between a pair of electrodes (Figure 1) is back-projected and recorded along the whole boundary of the body. This method is similar to X-ray computed tomographic (CT) reconstruction, with the main difference being that in EIT current does not move in a straight line but floods a region from source to drain. Although back-projection was very successful for simple 2D geometries, a number of deterministic algorithms based on the Jacobian (from boundary potential to internal conductivity) of the discrete forward solution have been introduced.

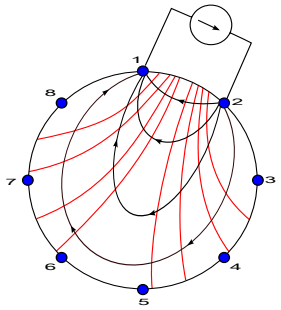

Figure 1: Likely equipotential lines (in red) for a circular 2D body with current injected through a pair of adjacent electrodes.

Compared with other imaging modalities (e.g. X-ray CT), EIT/ERT appears to be more challenging because the Jacobian that relates the interior conductivity perturbations to potential measurements at the electrodes is strongly ill-conditioned and small changes in the data can result in large and unpredictable changes in the reconstructed image.

The forward problem can be derived by solving the Laplacian elliptic partial differential equation

$$\sigma \nabla^2 u = 0 \tag{1}$$

with a mixed Dirichlet and Neumann boundary condition. The resulting forward problem is

$$\sigma \frac{\partial u}{\partial n} = -J_s \cdot n \equiv j \,, \tag{2}$$

where σ is the electrical conductivity, u is the electric

potential, n is the outward unit normal to the boundary ($\partial\Omega$) and j is the negative normal component of injected current density J_s, or simply the injected current.

A complete electrode model [Vauhkonen, 1997] considers the existence of a discrete number of electrodes of finite size. The measured potential V_l at the l'th electrode is equal to the sum of potentials over the boundary surface under the electrode, allowing for the electrode's contact impedance z_l. This model also states that the current density over the surface s of an electrode totals the current I_l through the electrode. The complete electrode model is

$$u + z_l \sigma \frac{\partial u}{\partial n} = V_l \quad x \in e_l, \quad l = 1, 2, ..., L \tag{3}$$

$$\int_{e_l} \sigma \frac{\partial u}{\partial n} ds = I_l \quad x \in e_l, \quad l = 1, 2, ..., L \tag{4}$$

$$\sigma \frac{\partial u}{\partial n} = 0 \quad x \notin e_l, \qquad l = 1, 2, ..., L\,. \tag{5}$$

In addition, to ensure the uniqueness of the solution the conservation of charge theorem must hold

$$\int_{\partial\Omega} j = 0 \quad \Rightarrow \quad \sum_{l=1}^{L} I_l = 0\,, \tag{6}$$

together with a choice of an arbitrary ground or reference voltage

$$\int_{\partial\Omega} u = 0\,. \tag{7}$$

2.1 Numerical approximation

A technique commonly used to solve the system of partial differential equations (1–5) is the finite element method (FEM). The method is based on transforming the continuous form of the problem into a discrete approximation constructed as a finite collection of K elements with constant conductivity interconnected through N nodes. Applying FEM theory [Silvester and Ferrary, 1983] and rearranging the finite element system of equations into a matrix representation leads to

$$\begin{bmatrix} A_M + A_Z & A_V \\ {A_V}^T & A_D \end{bmatrix} \begin{bmatrix} U \\ V_l \end{bmatrix} = \begin{bmatrix} 0 \\ I_l \end{bmatrix}, \tag{8}$$

where U is a vector of potentials at the N finite element nodes and

$$\begin{bmatrix} A_M + A_Z & A_V \\ {A_V}^T & A_D \end{bmatrix} \tag{9}$$

is known as the symmetric admittance matrix. This matrix associates each of the K elements with its constituent nodes and its conductivity. For more information the reader is referred to [Vauhkonen, 1997; Holder, 2005].

To complete the system, and ensure a unique solution, the forward model must include patterns of injected current

$$\boldsymbol{I}_l = \begin{bmatrix} I_1 & I_2 & ... & I_k \end{bmatrix}, \tag{10}$$

such that the current injected into the body equals the current sunk out.

2.2 Inverse solution and image reconstruction

Functional requirements for an artificial sensitive skin in robotics are debatable. It is clear, however, that integration of a skin over all or most of the surface of a robot's body will potentially improve the robot's capability for interaction through touch. To achieve this potential both data acquisition and interpretation algorithms must execute in real time.

Difference imaging or dynamic imaging [Adler and Guardo, 1996] is a fast, non-iterative method of imaging that reduces possible problems with unknown contact impedance and inaccurate electrode position [Lionheart, 2004]. The essence of the method is to first calculate the initial state of potentials $\boldsymbol{V}_l$ for an assumed *homogenous* body with 'known' conductivity $\boldsymbol{\sigma_0}$. The discrete model is then replaced by a linear approximation used to compute only the difference $\delta\boldsymbol{\sigma}$ from the *inhomogeneous* case. Then, after calculating the Jacobian $\boldsymbol{J}$ between changes in boundary potential and internal conductivity, the discrete form of the linearised problem becomes

$$\delta\boldsymbol{V}_l \approx \boldsymbol{J}\delta\boldsymbol{\sigma} + \boldsymbol{n}\,, \tag{11}$$

where $\boldsymbol{n}$ is a noise vector and $\delta\boldsymbol{V}_l$ is the difference in potential between two measurements: the homogenous and inhomogeneous cases.

Since little current passes through most of the elements, many values in the Jacobian will be close to zero. Dividing by such small values causes numerical sensitivity in the solution so that small changes in measured potentials can cause large changes in the reconstruction; this ill-posed problem has to be solved by regularisation.

Informally, regularisation means that additional information is introduced so that an ill-posed problem can be replaced by a nearby well-posed problem. For EIT the extra information is usually an assumption that $\delta\boldsymbol{\sigma}$ is slowly changing, smooth or 'blocky' [Kolehmainen *et al.*, 1997].

A widely used regularisation method is Tikhonov regularisation, in which the ill-conditioned problem

$$\delta\boldsymbol{\sigma} = \boldsymbol{J}^{-1}\delta\boldsymbol{V}_l \tag{12}$$

is replaced by

$$\delta\boldsymbol{\sigma} = (\boldsymbol{J}^T\boldsymbol{J} + \alpha\boldsymbol{R})^{-1}\boldsymbol{J}^T\delta\boldsymbol{V}_l\,, \qquad (13)$$

where α is a scalar hyperparameter that controls the amount of regularisation and $\boldsymbol{R}$ is a regularisation matrix that controls the smoothness of the solution.

For this study, the generalised Tikhonov regularisation as presented in [Adler and Guardo, 1996; Holder, 2005; Adler and Lionheart, 2006] is used; this solution has the form

$$\delta\boldsymbol{\sigma} = (\boldsymbol{J}^T\boldsymbol{W}\boldsymbol{J} + \alpha^2\boldsymbol{R}^T\boldsymbol{R})^{-1}\boldsymbol{W}\boldsymbol{J}^T\delta\boldsymbol{V}_l\,, \qquad (14)$$

where $\boldsymbol{W}$ is a weighting matrix and, for a fixed initial $\boldsymbol{\sigma}$, the Jacobian $\boldsymbol{J}$ and $(\boldsymbol{J}^T\boldsymbol{W}\boldsymbol{J} + \alpha^2\boldsymbol{R}^T\boldsymbol{R})$ can be precalculated off-line, greatly speeding up the solution.

3 Proposed EIT Method

Many different strategies of current injection and potential measurement—hereon termed 'drive patterns'—can be applied in EIT. Some drive patterns have previously been compared [Avis and Barber, 1994; Demidenko *et al.*, 2005; Shi *et al.*, 2006; Kaipio *et al.*, 2007; Xu *et al.*, 2008] with the aim of finding the drive pattern that provides the best resolution and performance in the presence of noise. The most commonly used strategy is the adjacent method, in which current is injected through a pair of adjacent electrodes and the potential is measured at all other adjacent electrode pairs (Figure 2). The electrical potential is typically not measured at electrodes containing injected current, so that for the adjacent method using 16 electrodes a total of 208 voltage measurements are obtained. Due to the reciprocity principle [Geselowitz, 1971] only half of these are independent, reducing the number of measurements to 104.

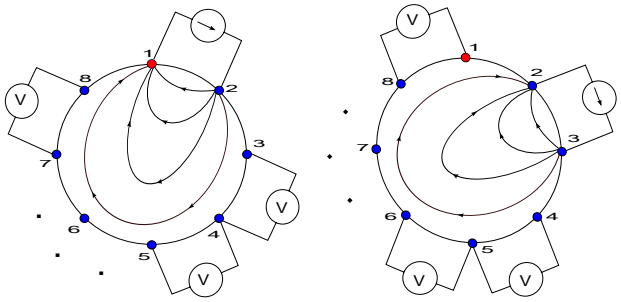

Figure 2: First (left) and second (right) steps for the adjacent drive pattern.

Although conclusive results are difficult to find because EIT image resolution depends strongly on the reconstruction algorithm and its parameters [Xu *et al.*, 2008], the present study attempts to eliminate any inconsistencies and compares a number of drive patterns which include the introduction of a reference electrode within the body's structure. Simulations were performed on different geometries with 16 electrodes on the boundary and a 17th electrode in different locations within the body. To avoid the 'inverse crime' two different FEM meshes were generated using distmesh© [Persson and Strang, 2004]. Since a sensitive skin should cover most of a robot's body, both circular and rectangular 2D shapes were used.

The point electrode method in which electrodes are considered to be single nodes in the mesh was used for all simulations. Contact impedances between electrodes and the 2D body were ignored. The Jacobian was calculated by solving the forward model for each element and the generalised Tikhonov regularisation method was applied for the inverse solution with $\boldsymbol{W}$ replaced by the identity matrix $\boldsymbol{I}$ and $\boldsymbol{R}^T\boldsymbol{R}$ modelled as a Gaussian high pass filter [Adler and Guardo, 1996]. A total of 563 elements connected by 313 nodes were used for the forward solution of the circular body and 545 elements with 311 nodes for the rectangular body. Finite elements and nodes for the rectangular body can be seen in Figure 3.

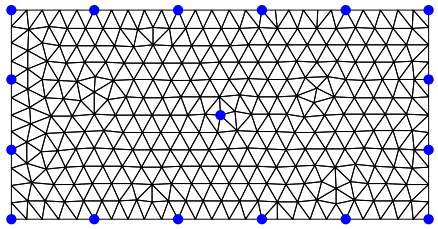

Figure 3: Finite element discretisation for a rectangular body with 17 electrodes, shown in blue.

Initial conductivity was set as 1 S/cm for the full body and each element of the mesh was stimulated in turn with a 10% conductivity increase to represent a localised touch. Since the characteristics of the noise are not expected to alter with changes to the drive patterns, fixed levels of Gaussian noise ranging from .05 to 35μV RMS were added to the simulated data at the 'measuring' points. These noise levels are typical values that can be achieved by over-sampling each measurement 15-20 times. Preliminary experimental testing (not reported here) used a stretchable conductive cloth manufactured by Less EMF Inc. To provide quantitative data characterising noise rejection, 200 reconstructions were performed for each element. The analysis presented here is based on the results (mean and standard deviation) for each stimulated element and the average of all elements in the mesh.

3.1 Current drive patterns

All simulations were performed by applying current (110mA) through a single pair of electrodes and taking

potential measurements at all other pairs. To achieve a constant dynamic range in the data, measurements were not taken from electrodes when they were used to inject current. Drive patterns were designed to test the influence of the relative position of the measurement electrodes to the current source and sink locations.

The current sink was initially located at the electrode adjacent to the source (adjacent method). Subsequently, the sink was progressively separated from the source one electrode at a time until the current source and sink electrodes were opposite to each other (180 degrees of separation or opposite method). These current excitation methods were named as '1' to '8' according to the number of electrodes of separation. Additionally, the sink electrode was located in a fixed position *inside* the conductive body; this excitation was named according to the location node or simply 'centre' if located in the centre of the geometry.

Measurement patterns were also rotated in the same way as current patterns to take measurements from different pairs of electrodes. If the centre node was used as a reference electrode, this was considered a 'centre measurement' pattern. Despite the reciprocity principle, all measurements were considered for image reconstruction.

3.2 Resolution and performance metrics

Assessing the quality of a reconstructed image in EIT can be misleading and complicated. Many different metrics have been used (and compared [Wheeler *et al.*, 2002]) in an attempt to find a metric that objectively measures the 'quality' of different reconstructions. In this section, four metrics are proposed with the aim of evaluating the quality of the reconstructed images when used in a sensitive skin application.

1, 2. *Resolution at 50% [or 75%] image amplitude.* We considered the resolution as a ratio of the number of elements containing 50% [or 75%] the maximum amplitude to the total number of elements in the mesh:

$$res = \left(1 - \sqrt{\frac{Elements\ over\ 50\%\ [75\%]}{Total\ Elements}}\right) * 100\,. \quad (15)$$

For 563 elements a resolution of of 95.78 represents best performance by this measure. As the resolution increases, so does the capability of the system to discriminate between two different stimuli.

3. *Resolution at negative 35% image amplitude.* The same method as in Equation (15) was used to determine if there were any elements that exceeded a 35% reduction of conductivity (opposite to that expected) from the maximum amplitude. A value of 100 results when no elements are found—perfect performance by this measure.

4. *Distance error at 75% image amplitude.* For a sensitive skin, the location of the stimulus can have a great influence on the interpretation of touch. It is therefore important to minimise the error on stimulus localisation. The distance error represents the system's ability to locate the centroid of the stimulus. A value of zero would represent perfect performance by this measure.

3.3 Hyperparameter selection

The hyperparameter α in Equation 14 controls a trade-off between a solution based on measured data and the imposed prior. Correct selection of this parameter is crucial to achieving 'good' reconstruction. A number of selection algorithms exist in the field of inverse problems such as the L-curve, generalised cross validation (GCV) and fixed noise figure (FN) [Adler and Guardo, 1996], but in EIT an heuristic selection is still very common.

Comparing different reconstruction algorithms can be subjective, complicated and inconsistent if heuristic methods are used. The above-mentioned methods were compared in [Graham and Adler, 2006], who introduced a new method of hyperparameter selection: the 'BestRes' method. This method was shown to be consistent in finding a 'good' reconstruction which, in principle, is similar to the 'best' heuristic choice. In the present study a similar method was implemented based on resolution and distance curves (Figure 4).

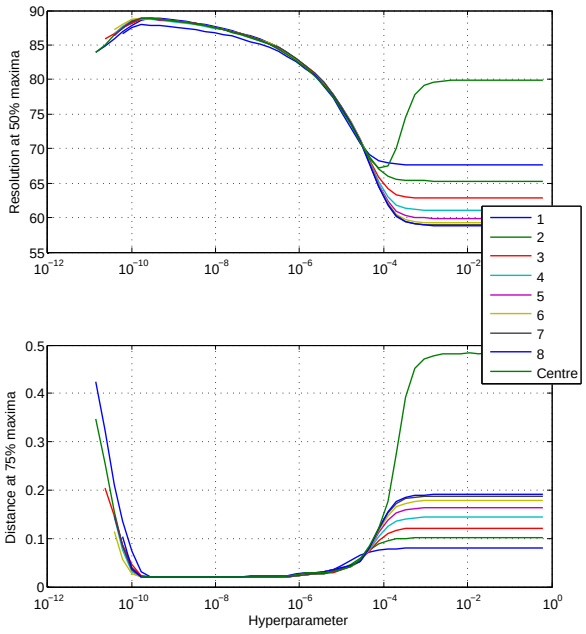

Figure 4: Resolution (top) and distance error (bottom) curves for a circular geometry, centre measurement pattern and nine current injection patterns.

These curves are the result of systematically reducing the hyperparameter to find the value at which the system has its best performance. The following method was used to create the resolution and distance curves:

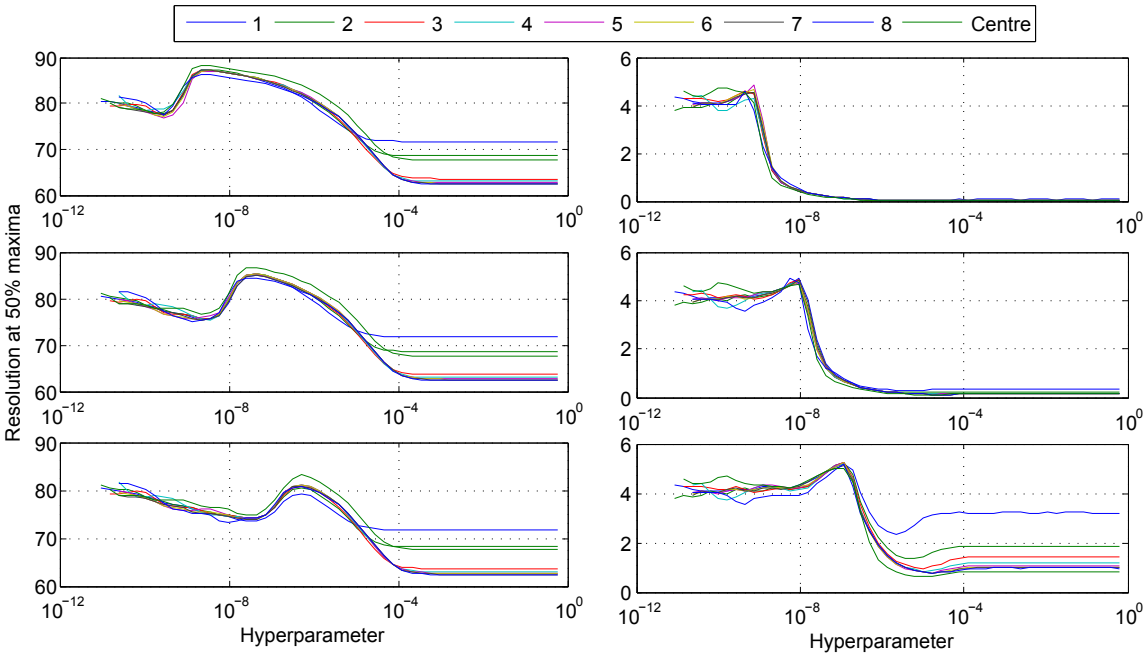

Figure 5: Resolution at 50% maxima. Mean (left) and standard deviation (right) curves for a circular geometry, adjacent measurement pattern and 9 current injection patterns with fixed Gaussian noise levels increasing from top (.07μV RMS) to bottom (7μV RMS). A total of 200 reconstructions were performed for each element.

1. Set the hyperparameter value initially to 1;
2. Solve the EIT system and reconstruct the image for all elements in the mesh;
3. Calculate the resolution and distance error metrics for each element as presented in Section 3.2;
4. Calculate mean and standard deviation for all elements in the mesh;
5. Reduce the hyperparameter and go to step 2.

It is important to recognise that some noise is to be expected in any practical EIT implementation such as a robotics sensitive skin. As shown in Figure 5, changing the hyperparameter also represents a trade-off between the resolution and performance in the presence of noise. As the value of the hyperparameter approaches unity, the resolution decreases but the robustness to measurement noise improves. Although good selection of the hyperparameter value is required, the resolution curves for all drive patterns are similar (Figure 5) so that precise selection of the hyperparameter value is not necessary when comparing drive patterns.

4 Simulation Results

Singular value decompositions (SVDs) of the Jacobian for all current excitation patterns were calculated, and normalised singular values for some of these drive patterns are presented in Figure 6. Plots show a rapid decrease between index 70 and 130 which confirms the ill-posedness of the system. The variations in divergence from the low to high singular value positions clearly shows that the 'opposite' drive pattern is the most ill-conditioned, confirming results obtained by Avis and Barber [1994].

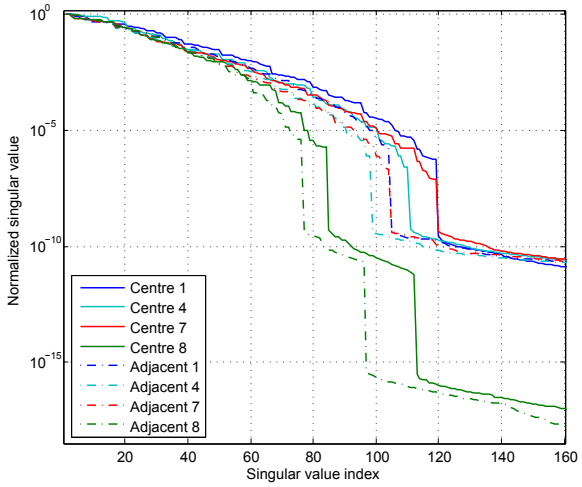

Figure 6: Normalised singular values of the Jacobian for a circular geometry and eight different drive patterns.

Resolution results (Figure 7) show the performance of different injection patterns for a fixed hyperparameter based on the best possible resolution without the addition of noise. These results demonstrate that including

a reference electrode in the centre of the geometry improves the resolution for all current excitation patterns. The reciprocity principle is also confirmed, since identical results are obtained if current excitation and potential measurement patterns are transposed.

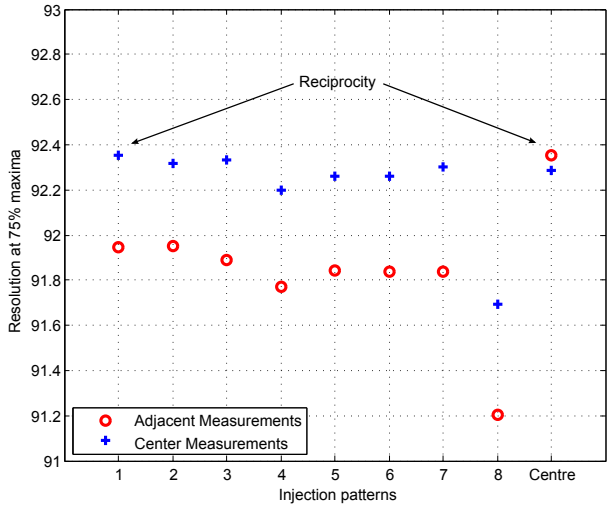

Figure 7: Resolution at 75% maxima for a circular geometry, adjacent and centre measurement patterns and nine current injection patterns.

Simulation results for image resolution with the addition of fixed levels of Gaussian noise (Table 1) confirmed the results obtained by Shi *et al.* [2006] who found that the adjacent method performs worst in the presence of noise while the 7th (pseudo-opposite) method has better performance than others. In addition, this result demonstrates that the performance of the system is still the best when an electrode is located in the centre of the body.

Table 1: Mean and standard deviation of resolution at 50% maxima for fixed hyperparameter and 7μV RMS noise in a circular geometry.

Pattern	Measurements			
	Adjacent		Centre	
	Mean	SD	Mean	SD
1	78.82	2.72	82.76	1.33
2	80.03	2.20	82.88	1.20
3	80.47	1.97	82.72	1.15
4	80.69	1.87	82.70	1.29
5	80.74	1.84	82.76	1.28
6	80.68	1.85	82.83	1.21
7	80.50	1.88	82.92	1.20
8	80.26	1.92	82.26	1.51
Centre	82.76	1.33	82.58	1.28

If we examine the performance of each element in the body, the best resolution and noise rejection is obtained near the boundary where most of the current flows. Figure 8 shows a comparison of the performance (mean and standard deviation) of each element with fixed hyperparameter and noise level. These results show that including an electrode in the centre of the geometry improves the response of the system particulary in the area where the worst performance was initially expected.

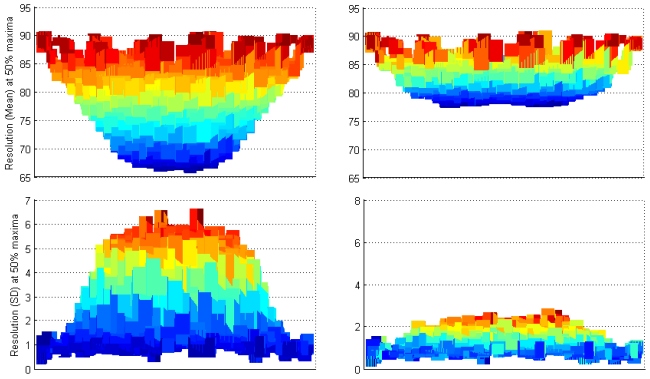

Figure 8: Lateral view of resolution at 50% maxima in a circular geometry and 7μV RMS noise. Adjacent (left column) and centre (right column) measurement patterns. Mean (top row) and standard deviation (bottom row) of all element in the mesh.

Reconstruction results presented in Figure 9 show the expected image for the same noise levels and conductivity changes in two different geometries if a single element is stimulated. Only the patterns of current excitation were changed from one reconstruction to the other.

5 Conclusions

The interpretation of touch is highly complex. When implementing an artificial sensitive skin for robotics, we need to take into account several requirements which are to some extent dependent on the robot's application. This work was focused in the development of a full-body sensitive skin based on EIT, with the main objective of contributing to improving robotic interaction through touch.

Electrical impedance tomography is an imaging technique in which the internal conductivity of a body can be estimated by using only measurements on its boundary. If this technique is applied in a thin, flexible and stretchable material that responds to touch with local changes in conductivity, an artificial sensitive skin can be created. Unfortunately, this is an ill-posed inverse problem in which small changes in the measurements can cause large unpredictable changes in the reconstruction; particulary in the centre of the body, where less current flows.

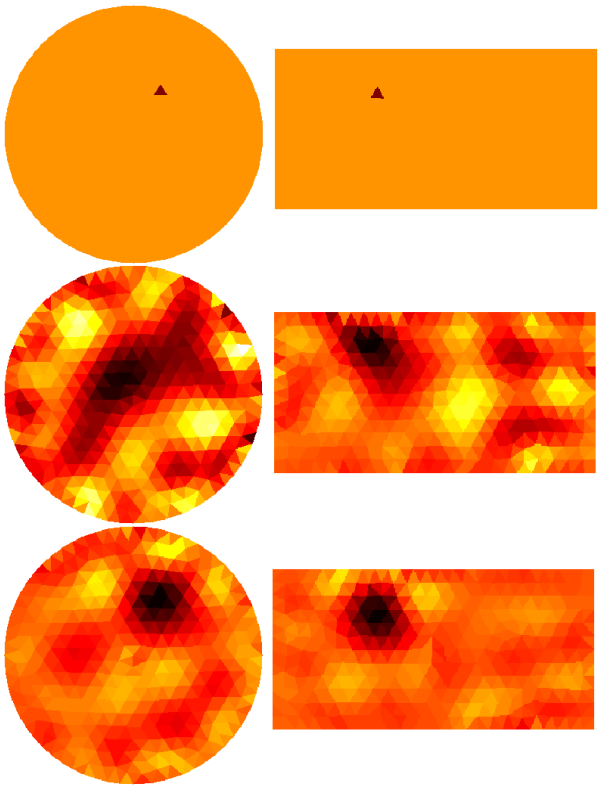

Figure 9: Reconstruction for different drive patterns with 7μV RMS noise. Stimulus (top), adjacent drive pattern (middle), adjacent injection pattern and centre measurement pattern (bottom).

It has previously been argued that in EIT the best resolution could be obtained by using the adjacent method, while an improved reconstruction in the presence of noise was achieved with the pseudo-opposite current injection pattern. This work has demonstrated, however, that adding a reference electrode in the centre of the geometry improves resolution, consistency along the body and reliability in the reconstruction. Furthermore, a centre reference for all voltage measurements simplifies hardware implementation and permits parallel measurements, hence reducing data acquisition times.

This paper also introduced a number of metrics that can be used to evaluate the performance of the EIT images in terms of location and resolution of a single stimulus. These metrics also characterise the ability to differentiate between stimuli applied to different locations on the sensitive skin.

Although tests were performed where reference electrodes were located in different places inside the body, the best resolution and robustness to noise was obtained with a reference electrode placed at the centre of the geometry, where the worst performance was initially expected.

Future work might be needed to locate the best position for the reference electrode in more complex geometries where performance needs to be improved in areas distant from the centre. In addition, a number of reference electrodes could be added to improve resolution in areas that have high aspect ratios.

References

[Adler and Guardo, 1996] A. Adler and R. Guardo. Electrical impedance tomography: regularized imaging and contrast detection. *IEEE Transactions on Medical Imaging*, 15(2):170–179, Apr. 1996.

[Adler and Lionheart, 2006] Andy Adler and William R B Lionheart. Uses and abuses of EIDORS: an extensible software base for EIT. *Physiological Measurement*, 27:S25–S42, 2006.

[Alirezaei *et al.*, 2009] H. Alirezaei, A. Nagakubo, and Y. Kuniyoshi. A tactile distribution sensor which enables stable measurement under high and dynamic stretch. *IEEE Symposium on 3D User Interfaces 2009*, pages 87–93, Mar. 2009.

[Avis and Barber, 1994] N J Avis and D C Barber. Image reconstruction using non-adjacent drive configurations. *Physiological Measurement*, 15:A153–A160, 1994.

[Barber *et al.*, 1992] D.C. Barber, B.H. Brown, and N.J. Avis. Image reconstruction in electrical impedance tomography using filtered back projection. *Proceedings of the Annual International Conference of the IEEE Engineering in Medicine and Biology Society*, 5:1691–1692, Oct. - Nov. 1992.

[Breazeal, 2003] Cynthia Breazeal. Toward sociable robots. *Robotics and Autonomous Systems*, 42:167–175, 2003.

[Chang *et al.*, 2006] W. Chang, K. E. Kim, H. Lee, J. K. Cho, B. S. Soh, J. H. Shim, G. Yang, S.-J. Cho, and J. Park. Recognition of grip-patterns by using capacitive touch sensors. In *IEEE International Symposium on Industrial Electronics*, volume 4, pages 2936–2941, 2006.

[Demidenko *et al.*, 2005] E. Demidenko, A. Hartov, N. Soni, and K.D. Paulsen. On optimal current patterns for electrical impedance tomography. *IEEE Transactions on Biomedical Engineering*, 52(2):238–248, Feb. 2005.

[Geselowitz, 1971] David B. Geselowitz. An application of electrocardiographic lead theory to impedance plethysmography. *IEEE Transactions on Biomedical Engineering*, BME-18:38–41, 1971.

[Graham and Adler, 2006] B M Graham and A Adler. Objective selection of hyperparameter for EIT. *Physiological Measurement*, 27:S65–S79, 2006.

[Heslin, 1974] R. Heslin. Steps toward a taxomony of touching, May 1974. Paper presented to the annual meeting of the Midwestern Psychological Association, Chicago, IL.

[Holder, 2005] David S Holder. *Electrical Impedance Tomography*. Institute of Physics Publishing, Bristol and Philadelphia, 2005.

[Hoshi and Shinoda, 2006] T. Hoshi and H. Shinoda. A sensitive skin based on touch-area-evaluating tactile elements. *Haptic Interfaces for Virtual Environment and Teleoperator Systems, 2006 14th Symposium on*, pages 89–94, Mar. 2006.

[Ishiguro and Nishio, 2007] Hiroshi Ishiguro and Shuichi Nishio. Building artificial humans to understand humans. *Journal of Artificial Organs*, pages 133–142, 2007.

[Kaipio *et al.*, 2007] Jari P Kaipio, Aku Seppnen, Arto Voutilainen, and Heikki Haario. Optimal current patterns in dynamical electrical impedance tomography imaging. *Inverse Problems*, 23:1201–1214, 2007.

[Kato *et al.*, 2007] Y. Kato, T. Mukai, T. Hayakawa, and T. Shibata. Tactile sensor without wire and sensing element in the tactile region based on EIT method. In *IEEE Sensors 2007*, volume 2, pages 792–795, Oct. 2007.

[Kolehmainen *et al.*, 1997] V. Kolehmainen, M. Vauhkonen, P.A. Karjalainen, and J.P. Kaipio. Spatial inhomogeneity and regularization in EIT. In *Engineering in Medicine and Biology Society, 1997. Proceedings of the 19th Annual International Conference of the IEEE*, volume 1, pages 449–452 vol.1, Oct-2 Nov 1997.

[Lionheart, 2004] William R B Lionheart. EIT reconstruction algorithms: pitfalls, challenges and recent developments. *Physiological Measurement*, 25:125–142, 2004.

[Lumelsky *et al.*, 2001] Vladimir J. Lumelsky, M.S. Shur, and S. Wagner. Sensitive skin. *IEEE Sensors Journal*, 1(1):41–51, Jun. 2001.

[McDaniel and Andersen, 1998] Ed McDaniel and Peter A. Andersen. International patterns of interpersonal tactile communication: A field of study. *Nonverbal Behavior*, 22:1, 1998.

[Minato *et al.*, 2007] Takashi Minato, Yuichiro Yoshikawa, Tomoyuki Noda, Shuhei Ikemoto, Hiroshi Ishiguro, and Minoru Asada. Cb2: A child robot with biomimetic body for cognitive developmental robotics. *7th IEEE-RAS International Conference on Humanoid Robots*, 1:557–562, 2007.

[Mori, 1970] Masahiro Mori. Bukimi no tani [The uncanny valley]. *Energy*, 7(4):33–35, 1970. In English: K. F. MacDorman and T. Minato (translate).

[Mukai *et al.*, 2008] T. Mukai, M. Onishi, T. Odashima, S. Hirano, and Zhiwei Luo. Development of the tactile sensor system of a human-interactive robot RI-MAN. *IEEE Transactions on Robotics*, 24(2):505–512, Apr. 2008.

[Mukat, 2004] T. Mukat. Development of soft areal tactile sensors for symbiotic robots using semiconductor pressure sensors. *Proceedings of ROBIO 2004. IEEE International Conference on Robotics and Biomimetics*, pages 96–100, Aug. 2004.

[Nagakubo *et al.*, 2007] A. Nagakubo, H. Alirezaei, and Y. Kuniyoshi. A deformable and deformation sensitive tactile distribution sensor. *Proceedings of ROBIO 2007. IEEE International Conference on Robotics and Biomimetics*, pages 1301–1308, Dec. 2007.

[Nicholls, 1991] H.R. Nicholls. Tactile sensing for robotics. *IEE Colloquium on Robot Sensors*, pages 5/1–5/3, Jan. 1991.

[Papakostas *et al.*, 2002] T.V. Papakostas, J. Lima, and M. Lowe. A large area force sensor for smart skin applications. *Proceedings of IEEE Sensors 2002*, 2:1620–1624, 2002.

[Persson and Strang, 2004] Per-Olof Persson and Gilbert Strang. A simple mesh generator in matlab. *SIAM Review*, 46:2, 2004.

[Shi *et al.*, 2006] Xuetao Shi, Xiuzhen Dong, Wanjun Shuai, Fusheng You, Feng Fu, and Ruigang Liu. Pseudo-polar drive patterns for brain electrical impedance tomography. *Physiological Measurement*, 27:1071–1080, 2006.

[Shimojo *et al.*, 2004] M. Shimojo, A. Namiki, M. Ishikawa, R. Makino, and K. Mabuchi. A tactile sensor sheet using pressure conductive rubber with electrical-wires stitched method. *IEEE Sensors Journal*, 4(5):589–596, Oct. 2004.

[Silvester and Ferrary, 1983] P.P. Silvester and R.L Ferrary. *Finite Elements for electrical engineers*. University of Cambridge, 1983.

[Someya *et al.*, 2006] T. Someya, T. Sakurai, and T. Sekitani. Large-area electronics based on organic transistors. *64th Device Research Conference*, pages 209–210, Jun. 2006.

[Stiehl and Breazeal, 2005] Walter Dan Stiehl and Cynthia Breazeal. Affective touch for robotic companions. *Proceedings of Affective Computing and Intelligent Interaction (ACII-05)*, 3784:747–754, 2005.

[Stiehl and Breazeal, 2006] Walter Dan Stiehl and Cynthia Breazeal. A sensitive skin for robotic companions

featuring temperature, force, and electric field sensors. *Proceedings of IEEE/RSJ 2006. International Conference on Intelligent Robots and Systems*, pages 1952–1959, Oct. 2006.

[Vauhkonen, 1997] Marko Vauhkonen. Electrical impedance tomography and prior information. PhD thesis, 1997.

[Velonaki *et al.*, 2005] M. Velonaki, D.C. Rye, S.J. Scheding, and S.B. Williams. Fish-bird: Autonomous interactions in a new media arts setting. In *Proceedings of Vital Signs*, 2005.

[Wada *et al.*, 2002] K. Wada, T. Shibata, T. Saito, and K. Tanie. Analysis of factors that bring mental effects to elderly people in robot assisted activity. *Proceedings of IEEE/RSJ 2002. International Conference on Intelligent Robots and System*, 2:1152–1157, 2002.

[Wheeler *et al.*, 2002] James L Wheeler, WeiWang, and Mengxing Tang. A comparison of methods for measurement of spatial resolution in two-dimensional circular EIT images. *Physiological Measurement*, 23:169–176, 2002.

[Xu *et al.*, 2008] Canhua Xu, Xiuzhen Dong, Xuetao Shi, Feng Fu, Wanjun Shuai, Ruigang Liu, and Fusheng You. Comparison of drive patterns for single current source EIT in computational phantom. In *Proceedings of ICBBE 2008. The 2nd International Conference on Bioinformatics and Biomedical Engineering.*, pages 1500–1503, May 2008.

[Yohanan *et al.*, 2005] Steve Yohanan, Mavis Chan, Jeremy Hopkins, Haibo Sun, and Karon MacLean. Hapticat: Exploration of affective touch. *Proceedings of ICMI'2005. International Conference on Multimodal Interfaces*, pages 222–229, 2005.